Int J Adv Manuf Technol (2016) 82:1115–1125
DOI 10.1007/s00170-015-7392-8

ORIGINAL ARTICLE

Research on dynamic characteristic of softness consolidation abrasives in machining process

Xi Zeng[1] · Shi-ming Ji[1] · Ming-sheng Jin[1] · Da-peng Tan[1] · Jiang-qin Ge[1]

Received: 12 March 2015 / Accepted: 3 June 2015 / Published online: 30 June 2015

Abstract Pneumatic wheel based on softness consolidation abrasives (SCA) is presented as a key machining tool mainly for the improvement of finishing efficiency to free-form surface of laser-hardened molds. In this case, though its softness fits for machining to free-form surface, it cannot keep all abrasives within bounds strictly, but it makes abrasives experience creep deformation, which always leads to unstable machining characteristics. For research on the working rule of SCA, dynamic characteristics of abrasives need to be investigated. Firstly, soft ball model is brought into analysis of the normal and shear contact forces between two particles. By introducing damping coefficient, formulas on displacement and velocity of SCA are given for theory analysis of creep deformation. After that, force chains are established by simulation, which proves that SCA possesses more cutting force than free abrasives. At the same time, creep deformation of SCA is confirmed in accordance with the analysis of velocity of the single particle. Subsequently, combined with the modified Preston formula, comparative machining tests on material removal are carried on a laser-hardened free-form surface. Experimental results show that material removal rate of SCA is higher than that of free abrasive by approximately 34.35 %. Moreover, abrasive size is discussed as a key parameter respectively according to consolidation effects and surface roughness. The final conclusion is that SCA is certified to improve finishing efficiency for laser-hardened surfaces as well as suitable for machining free-form surfaces.

Keywords Laser-hardened mold · Machining · Creep deformation · Material removal · Softness consolidation abrasives

✉ Xi Zeng
franckie@126.com

Shi-ming Ji
jishiming@zjut.edu.cn

Ming-sheng Jin
jinmingsheng@zjut.edu.cn

Da-peng Tan
tandapeng@zjut.edu.cn

Jiang-qin Ge
1014840079@qq.com

[1] Key Laboratory of Special Purpose Equipment and Advanced Manufacturing Technology Ministry of Education, Zhejiang University of Technology, No. 18, Chao-wang Road, Hangzhou 310014, China

1 Introduction

In mold industry, laser-hardened method can not only significantly improve surface hardness, wearing resistance, and corrosion resistance, but can also optimize performance of mold steel and extend its service life. Qunli and Wang present the improvement of surface performance by simulations and experiments in laser cladding process [1, 2]. Hong reports microstructure and properties of steel in laser remelted and aging treatment [3]. Dandekar claims that sub-surface damage in laser-assisted machining can be predicted by multi-scale modeling [4]. What is more, certain part of surface could be extraordinarily strengthened according to specific demands, and thus, noble metal for mold manufacture could be economized enormously. Kwok proves that laser melting on a certain part of surface could improve wearing and corrosion resistance of mold steel [5]. Torkamany presents the excellent effect of laser welding on a local part of mold steel, especially in microstructure and mechanical performance [6]. All the findings above show that laser-hardened methods are playing important role in mold manufacturing gradually. However, these advantages

have also brought tremendous difficulties to the finishing process of laser-hardened surfaces, which is mainly reflected in the following three aspects: (1) Bonnet polishing method prevails in current finishing process with free abrasives, while freely moving abrasives have difficulties in efficiently machining surfaces of high hardness and high wearing resistance reported by Zeng [7]. (2) In finishing process to free-form surface, Yao shows that rigid grinding tool is formidable to contact properly with some irregular surfaces of workpiece, which can guarantee highly efficient processing [8]. But Sousa shows that abrasive configuration on the grinding process is not fit for finishing process to irregular surfaces of workpiece due to limitation of shape and size of tools [9]. (3) Currently, manual operation is widely used in dealing with locally deformed surfaces of high hardness, high wearing resistance, and difference in hardness, but it is difficult to handle with proper cutting force and dwell time in designated parts, which may lead to instable machining accuracy and low efficiency.

A number of scholars have put forward the following processing methods: Wu reports that belt grinding possesses high processing efficiency and enough softness to fit for free-form surface [10], and Song presents an adaptive modeling method for a robot belt grinding process [11]. But its structural deficiency constraints copying capacity to irregular surfaces in all directions, and the grinded surface still needs additional lapping and polishing till meeting accuracy requirement. Tsuneo focuses on EDM and ECM/ECM-lapping complex machining technology in lapping process [12], and Chiou presents a novel method of composite electroplating on lap in lapping process [13]. However, it works well only in the case of good match between lapping tool and the surface. Polishing reported by Shi and Han [14, 15] mainly adopts a flexible tool in conjunction with free abrasives, and Ji brings bonnet polishing technique into mold steel manufacturing [16]. But it can hardly suit for high-efficiency processing of laser-hardened surface owing to its low material removal capacity. Other scholars hold that such methods as abrasives flow and abrasives liquid jet can be applied to process free-form surface. Kuriyagawa presents electrorheological fluid-assisted polishing for small three-dimensional parts [17]. Suni reports rheological characterization of magnetorheological polishing fluid [18]. Das analyzes magnetorheological abrasive flow finishing process [19]. They all focus on fluid control processes. However, to an irregular workpiece, it is not easy to establish efficient flow passage or control fluid form for designated laser-hardened surfaces.

Despite that bonnet polishing leads to mirror-level processing effects, its low material removal cannot apply to laser-hardened surfaces of high hardness. In allusion to the difficulties mentioned above, we carried out researches on a kind of pneumatic wheel tool based on softness consolidation abrasives (SCA), aiming to rapidly reduce average roughness (R_a) from 0.4~0.6 to 0.06~0.09 μm as initial finishing process, and aiming to facilitate further mirror-level processing and thereby enhance automatic level and processing efficiency in the whole finishing process.

2 Design on SCA

Pneumatic wheel with SCA is mainly characterized by the following aspects: abrasives are consolidated on the outside surface of hemispherical rubber bonnet by the polymer binder. Meanwhile, softness of SCA is controlled by internal air pressure so that the pneumatic wheel could enjoy both copying capacity of bonnet polishing and cutting capacity of rigid wheel. Figure 1 shows contact between pneumatic wheel and workpiece and key influence factors. θ is tilting angle, R is radius of wheel, d is feeding depth, and h is diameter of contact area. All of the above have been reported by Zeng already [20].

In a macroscopic view, abrasives consolidated on the outside surface of hemispherical rubber bonnet are not as free as those abrasives in polishing process. But in a microscopic view, each abrasive acquires elastic support from the binder all around. When an abrasive is given a force, it will form a local micro-motion which may affect the surrounding abrasives to create force effect of groups. Figure 2 presents the deformation process of each abrasive from the microscopic point of view.

When normal force made the binder to deform, abrasives turn out to be compressive in a macroscopic view. After that, when tangential force is exercised, abrasives start to slide on the surface of mold. Due to the elastic support from binder, the contacting condition of abrasives varies according as binder's deformation. This characteristic enables abrasives to be more efficient and to achieve a stable cutting force. In comparison to

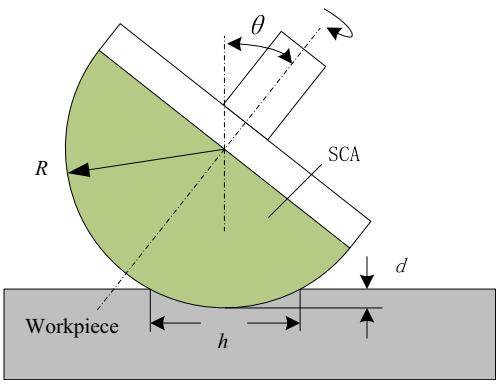

Fig. 1 Contact between pneumatic wheel and workpiece and key influence factors

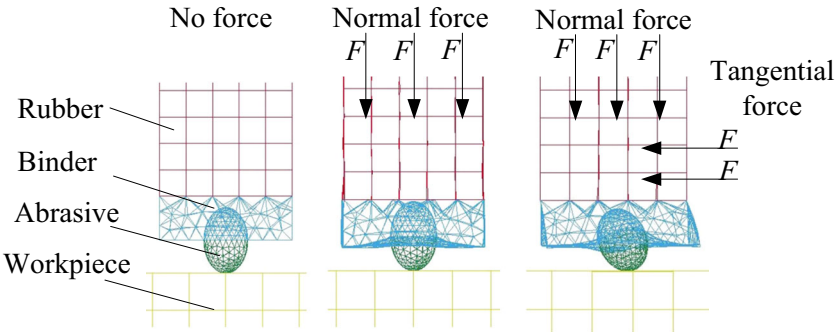

Fig. 2 Deformation processes of abrasives under normal and tangential force

free abrasive, processing efficiency of surfaces with high hardness and high wearing resistance could be enhanced. Moreover, elastic support of SCA and their dynamic constraint status not only ensure certain cutting force but also keep deep-scratches away.

The thickness of SCA as an important factor has a relationship with the cutting force. Different thickness of SCA means different mount of abrasives consolidated by the binder on outer layer of wheel. In force passing process from given force to final cutting force, it would form a temporary and stable force chain among abrasive particles [7]. So, the dynamic characteristics of SCA need to be discussed for machining results.

3 Characteristics analysis on SCA

3.1 Mechanics in SCA

According to Fig. 3, SCA generally appear to be a dense particle system accompany with particles constraining each other. The contacts between particles cannot happen instantaneously, but last for a while, which means several particles may contact with each other spontaneously within a system. At this moment, force amid particles serves as the key factor determining deformation and flowing of particles system. Therefore, soft ball model is adopted to help us acquire plenty of dynamic information of force among particles. Figure 3 shows normal contact model and tangential contact model of two abrasives [21].

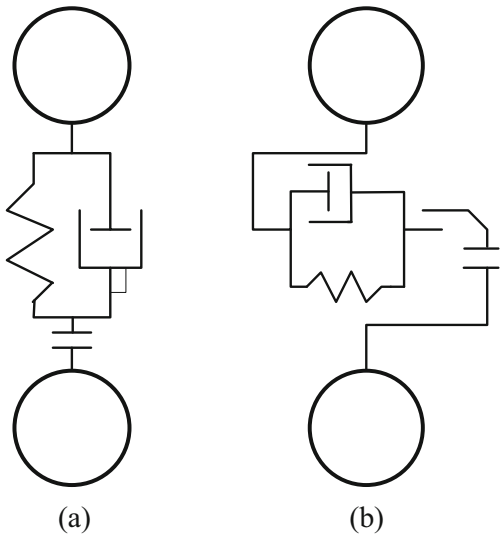

Fig. 3 Normal contact model (**a**) and tangential contact model (**b**) between two abrasives

When two abrasives collide against each other, their kinetic energy is consumed via interior friction, elastic wave and deformation. The normal contact model of this kind of mutual effects can be illustrated by the introduction of linear spring and damper on the contact point between two abrasives. In the process of machining, abrasive contact resulted from interior movement of SCA is illustrated by the models above.

In the normal contact model displayed in Fig. 4a, normal force of two abrasives "i and j" (i, j) is shown as:

$$F_{n,ij} = \begin{cases} -k_n \delta_{ij} n_{ij} - d_n v_{n,ij} & \delta_{ij} > 0 \\ 0 & \delta_{ij} \leq 0 \end{cases} \quad (1)$$

Where $F_{n,ij}$ is normal force, k_n is rigid coefficient of normal contact, δ is overlapping thickness of abrasives, d_n is normal

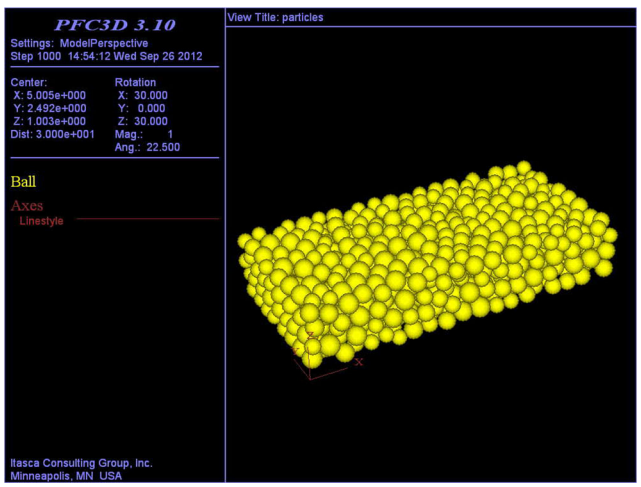

Fig. 4 SCA sample

Table 1 Parameters of sample abrasives

Length L/mm	Width W/mm	Height H/mm	Diameter d_p/mm	Number N	Coefficient μ
10	5	2	0.3	750	0.18

damping coefficient, $v_{n,ij}$ is normal relative velocity, and n_{ij} is normal unit vector.

If particles in SCA begin to contact continuously and tend to move without mutual relative slide, Mohr–Coulomb rule fails to work and tangential force is obviously smaller than sliding friction force. In addition, friction between particles will also lead to energy consumption in tangential direction, which could be calculated by adding a damper in tangential direction. The tangential force formula is given as:

$$F_{t,ij} = \min\left(-k_t\delta_t - d_t v_{t,ij}, k_f \left| F_{n,ij} \right| t_{ij}\right) \tag{2}$$

Where $F_{t,ij}$ is tangential force, k_t is rigid coefficient of tangential contact, $v_{t,ij}$ is tangential relative velocity, d_t is tangential damping coefficient, t_{ij} is tangential unit vector, and k_f is slide friction coefficient.

The analysis of normal force and cutting force among abrasives provides a theoretical basis for research on force chain of SCA.

3.2 Creep deformation of SCA

Without force, SCA are considered in the relaxation phase I, in which abrasives bonded by a binder constitute a layer without compression. When the layer is compressed, abrasives begin to have creep deformation and contact with each other. And then they form a relative balance. Here follows the relaxation phase II. According to dynamic relaxation method, the formula of critical damping oscillation is gradually integrated. Quality damp and rigid damp are utilized to absorb kinetic energy of the system. When damping coefficient is slightly smaller than a critical value, vibration of the system will disappear as fast as possible, with the function converging at a value at the same time.

The movement formula of i_{th} abrasive at time t is shown in equation (3), equation (4) and equation (5).

$$F_i(t) = m_i \frac{\dot{\mu}\ (t) - \dot{\mu}\ (t-\Delta t)}{\Delta t} + \beta\ \dot{\mu}\ (t) \tag{3}$$

Where $F_i(t)$ is force of i_{th} abrasive at time t, β is global damp system, m is abrasive weight, Δt is increment of time, and $\dot{\mu}\ (t)$ is acceleration formula.

$$\dot{\mu}\ (t) = \frac{1}{m_i + \beta\Delta t}\ \dot{\mu}\ (t-\Delta t) + \frac{\Delta t \cdot F_i(t)}{m + \beta\Delta t} \tag{4}$$

$$M_i(t) = I_i \frac{\dot{\theta}_i(t) - \dot{\theta}_i(t-\Delta t)}{\Delta t} + \beta\dot{\theta}_i(t) \tag{5}$$

In equation (5), $M_i(t)$ is rotational inertia of i_{th} abrasive at time t and $\dot{\theta}_i(t)$ is formula of angular acceleration.

$$\dot{\theta}_i(t) = \frac{1}{I_i + \beta\Delta t}\dot{\theta}_i(t-\Delta t) + \frac{\Delta t \cdot M_i(t)}{I_i + \beta\Delta t} \tag{6}$$

Translational displacement $\mathbf{S}(t)$ and rotational displacement $\mathbf{Q_i}(t)$ are shown as follows:

$$S(t) = S(t-\Delta t) + \dot{\mu}\ (t-\Delta t) \cdot \Delta t \tag{7}$$

$$Q_i(t) = Q_i(t-\Delta t) + \dot{\theta}_i(t-\Delta t) \cdot \Delta t \tag{8}$$

3.3 Material removal characteristics

When flexible bonnet provides force, there exist different cutting force between pneumatic wheel of SCA and rigid wheel of fixed abrasives. At this point, traditional Preston equation cannot precisely describe material removal characteristics of SCA [7].

Focusing on characteristics of SCA, combined with Rabinoweizc's theory firstly cited from Ji [22], modified Preston equation concluded by Zeng [7] is presented to describe material removal characteristics of SCA, as is shown in the following:

$$M_r = K' F^{2/3} v \tag{9}$$

Table 2 Parameters on bond strength of abrasives

Group	Normal rigid coefficient k_n	Tangential rigid coefficient k_t	Normal damping coefficient d_n	Tangential damping coefficient d_t
A	1×10^8	1×10^8	0	0
B	1×10^8	1×10^8	1.5×10^5	1.5×10^5
C	1×10^8	1×10^8	3.5×10^5	3.5×10^5
D	1×10^8	1×10^8	5.0×10^5	5.0×10^5

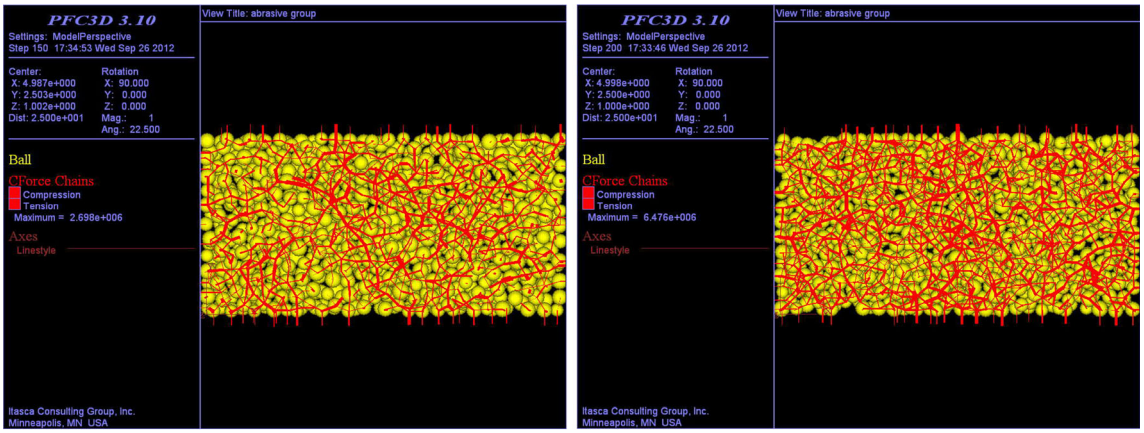

Fig. 5 Force chains of group *B* (**a**) and group *D* (**b**)

Where M_r is material removal rate, F is force on the surface, v is velocity of abrasives, and K' is modified coefficient, which as reported by Ji could be expressed as follows [23].

$$K' = \frac{D(d_p)H_p}{H_f} \tag{10}$$

Where $D(d_p)$ is coefficient decided by d_p, H_p is hardness of abrasives, and H_f is surface hardness of workpiece.

Modified Preston equation contributes to explaining relationship between cutting force and material removal rate. It verifies the credibility of mechanical analysis of SCA and can be used for optimization of processing parameters.

4 Numerical stimulation on SCA

4.1 Force chain

Firstly, it is necessary to build up a micro model of SCA in the stimulation of sample abrasives processing, with relevant parameters assumed in Table 1. The SCA sample is established by PFC3D, as shown in Fig. 4. All parameters are given according to real experimental parameters. Due to main research target focusing on dynamic characteristic of SCA, the shape of abrasives can be considered as spherical model in PFC3D.

In soft ball model, to avoid the calculation error caused by abrasive wearing, contact overlapping depth of particle is confined as $\delta_{max} \leqq 3\ \% d_p$. In line with parameters in Table 2 reported by Ji [23], force chains of SCA are simulated with normal force and tangential force.

Set d as 1 mm. The bond strength of abrasives is described by changing damping coefficient. Figure 5 shows force chains of group *B* and group *D* under the different damping coefficients.

Bond strength, mainly affected by volume fraction of abrasives and attribute of binder, can be switched to form corresponding force chain to match with processing requirements to free-form surface. In the process of transmitting force, the simulation results universally represent that the bigger damping coefficient in group *D* leads to the denser force chain distribution and the stronger contact force of abrasives in comparison with group *B*. This characteristic can be utilized to improve machining efficiency to local region of high hardness. In the process of being compressed, plenty of free abrasives like in group *A* are prone to escape (abrasives without any cutting effect). And force chain fails to converge for cutting and energy has to be consumed gradually along with abrasives' exfoliation from SCA.

Under the experimental conditions mentioned above, force simulation on a single particle Q selected from sample abrasives is conducted which is shown in right column of Table 3. According to equation 1 and equation 2, results are shown in middle column of Table 3.

By comparison, it can be found that simulation results are always lower than theoretical results, which is attributed to change of relative velocity caused by abrasives' creep deformation. As a consequence, calculation error can be controlled within 1 % and theoretical model may be applied for explaining creep deformation.

Table 3 Analysis on force of particle Q

Group	Theoretical force F/N	Simulated force F'/N
B	0.142×10^{-4}	$0.135\times10^{'4}$
C	$0.503\times10^{'4}$	$0.498\times10^{'4}$
D	$1.203\times10^{'4}$	$1.196\times10^{'4}$

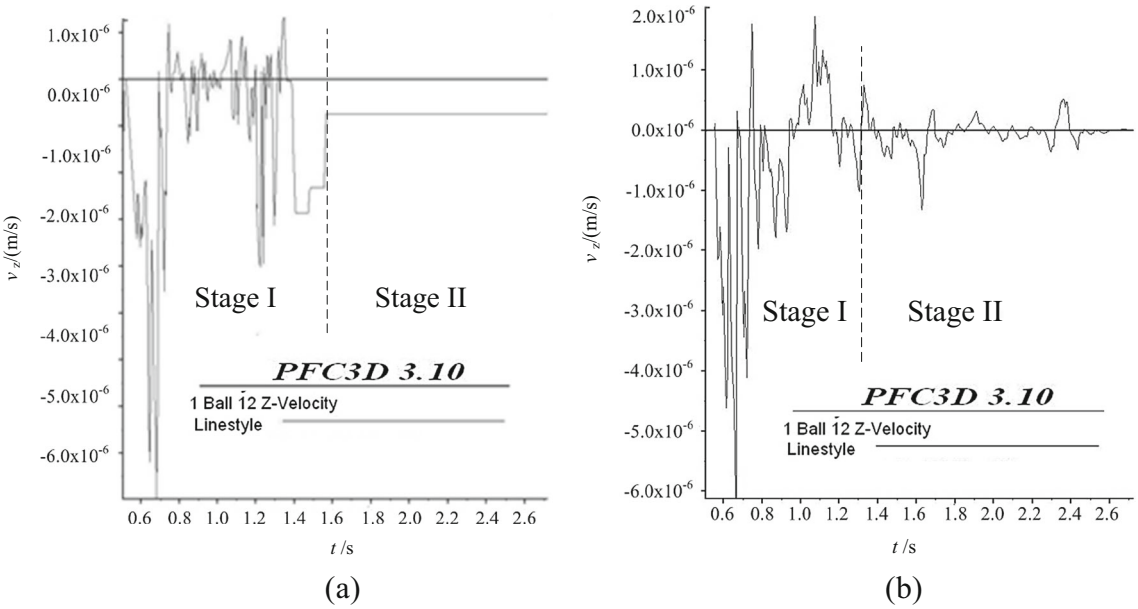

Fig. 6 Simulated velocity in direction of the axis *z* of free abrasives (**a**) and SCA (**b**)

4.2 Creep deformation of SCA

In a macroscopic view, the movement of SCA keeps pace with pneumatic wheel. However, in a microscopic view, rapid alteration of binder (tension or compression) triggers changes of displacement between particles, which causes abrasives' creep deformation.

The movement of abrasive can be divided into two stages: in stage I, abrasives are compressed and the statement of whole system turns from relaxation to tension; and in stage II, when abrasives are moving at a certain speed, SCA alter from a static balance to a new dynamic balance. This process has also been simulated for discussion. Set rotational speed (ω) of pneumatic wheel as 500 mm/s and the feeding depth (d) as 1 mm. For a better observation of creep deformation, machining area comprised of axis x and axis y is established and take v_z (velocity in direction of axis z) of particle P. Simulations on free abrasives and SCA are respectively carried out, as shown in Fig. 6.

Figure 6a shows V_z of particle P in direction of axis z. In stage I, V_z shows intensely variation and fluctuation. And then it appears to be stable at the end of stage I by degrees. Entering into stage II, V_z keeps a certain value all the time. That means that particle P has escaped from free abrasives group and it cannot be used for cutting any more. Figure 6b shows V_z of particle P in SCA. In stage I, it keeps variation and fluctuation as Fig. 6a. When it enters into stage II, V_z of particle P fluctuates around 0. That means particle P is under the constraint of bond. This creep deformation phenomenon manifests that

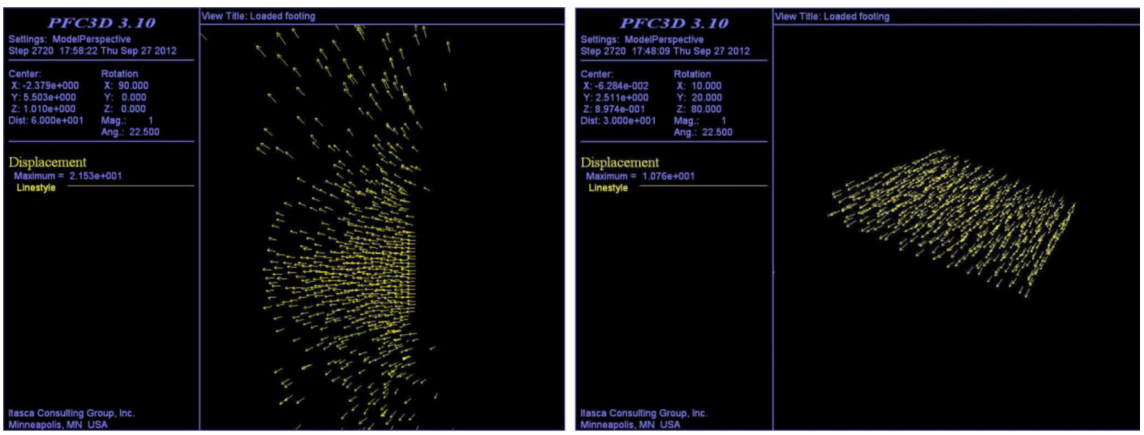

Fig. 7 Displacement of free abrasives (**a**) and SCA (**b**)

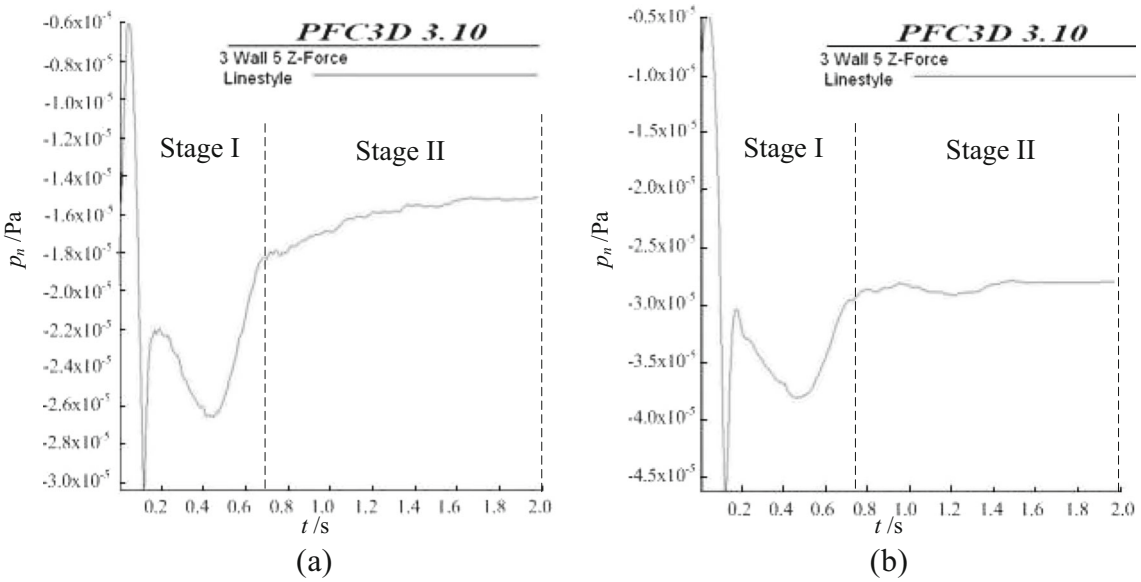

Fig. 8 Cutting force curves of free abrasives (**a**) and SCA (**b**)

particle P will always play a role for cutting and it will be adjusted according to contact gesture between pneumatic wheel and workpiece.

4.3 Analysis of cutting force

Figure 7 shows the displacements simulation results of SCA and free abrasives in machining process.

Without constraints, free abrasives are prone to escape from system as shown in Fig. 7a, which weakens cutting force for material removal. However, due to constraints to abrasives from binder, SCA can ensure concentrated cutting force to a given region of surface as shown in Fig. 7b. Creep deformation of abrasives causes effective compression to outer layer abrasives. Figure 8 shows the simulated cutting force curve of free abrasives and SCA.

Generally speaking, in stage I, cutting force increases rapidly until there is a static balance. In stage II, force reduces slightly and stays in a certain range until reaching a dynamic balance. Under the simulation conditions above, average pressure intensity of free abrasives to surface finally keeps a value of approximately 0.16 MPa (Fig. 8a), while that of SCA eventually maintains a value of approximately 0.26 MPa (Fig. 8b).

Through the simulation analysis above, we may draw a conclusion that force chain of abrasive could be enhanced by changing intensity of bonding to form concentrated force for higher-efficient machining. According to the analysis on a single particle, the credibility of theoretical model is confirmed. By our simulation researches on both micromovement and macromovement of particles, creep deformation of SCA which happens in machining process has been confirmed. This characteristic can be used for highlighting the benefits of an enhanced cutting force of abrasives.

Table 4 Machining parameters

Parameters	Value
Feeding depth d/mm	1
Tilting angle θ/°	30
Rotational velocity ω/mm/min	50
Diameter D_p/μm	75
Gas pressure p/Mpa	0.1
Rubber	SBR
Abrasives particles	Silicon carbide

Table 5 Different parameters among free abrasives, fixed abrasives, and SCA

Parameters	Free abrasives	Fixed abrasives	SCA
Damping coefficient	0	–	1.5×10^5
Abrasives consolidation method	No constraint	Laser sintering	Stocked with silicone sealant

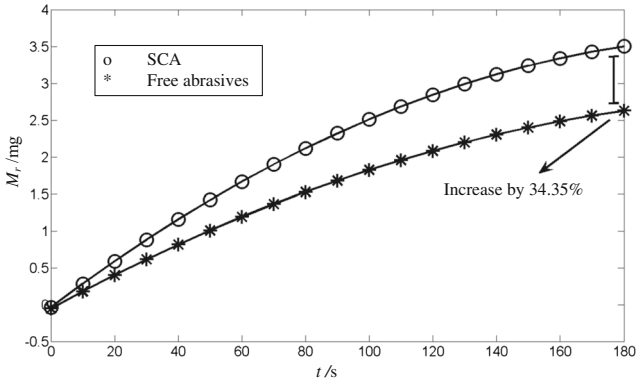

Fig. 9 Comparison of material removal rate between SCA and free abrasives

5 Experiment and discussion

5.1 Compositions of the machining system

Components of SCA machining system has been reported in our previous papers which mainly present machining process of SCA [7, 20]. The pneumatic wheel is fixed on the end of robot arm. The industrial robot MOTOMAN-HP20 is employed to control machining pneumatics wheel. The positioning accuracy of the robotic arm is in range of −0.06 to 0.06 mm. Especially, it has wide sphere of activity enough to fit for finishing large molds. This system can make full use of assisting advantages of robot and effectively overcome the shortcomings of manual polishing, such as poor working environment, low efficiency, and instable quality.

5.2 Machining effects

The empirical parameters are listed in Tables 4 and 5. The workpiece is made of die steel which has been hardened by laser with the hardness of 434 HV.

Figure 9 showed curves of material removal in a 3-min machining with free abrasives (bonnet polishing) and SCA (soft grinding). The dates were measured by precise electronic balance whose accuracy is 0.1 mg. In the machining process, material removal capacity of these two methods above showed a downward trend with t gradually because free abrasives cutting capacity decreased with plenty of abrasives running away and some abrasives in SCA were worn away and blunt gradually. However, it could be found that material removal of SCA is higher than that of free abrasives by approximately 34.35 %.

Obviously, SCA machining possessed higher material removal capacity than free abrasives over process time. This characteristic made SCA machining suitable for dealing with high hardness surface. Focus was also given to the surface roughness. Subsequently, comparative machining trials to curved surface were carried out respectively with free abrasives, fixed abrasives (grinding), and SCA by utilization of the parameters listed in Table 4. Machining time was set as 1 min, and

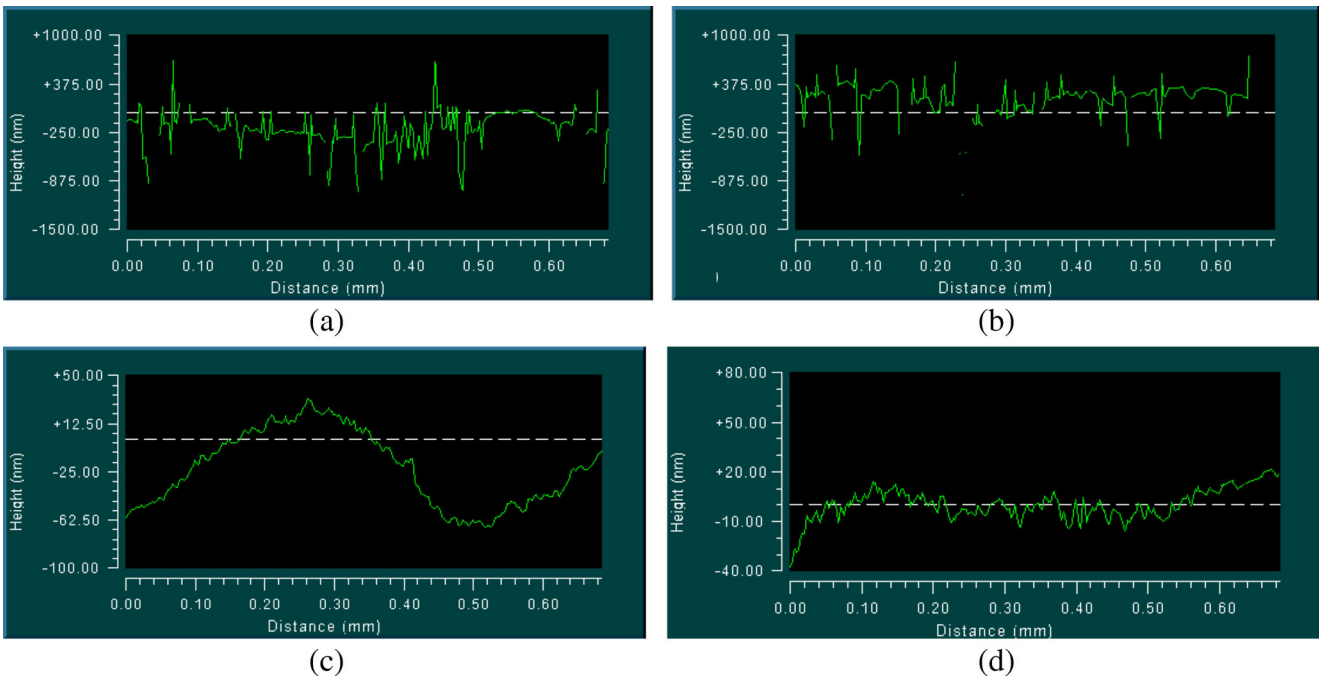

Fig. 10 Comparison on machining effects: initial surface (**a**), machining with free abrasives (**b**), machining by fixed abrasives (**c**), and machining by SCA (**d**)

Table 6 Particle size

Experimental group	Diameter D/μm
A	15
B	38
C	75
D	124
E	150
F	178

processed area was a circle. Roughness of surface was recorded by ZYGO as shown in Fig. 10.

Comparative machining trials were asked to deal with initial surface as shown in Fig. 10a. Obviously, processing result with free abrasives did not show improvement of roughness in Fig. 10b. Its weak cutting ability led to low machining efficiency, especially when it faced with high surface hardness. Figure 10c indicated that rigid wheel with fixed abrasives failed to adapt to complicated curvature surface whose partial areas were excessively embedded by abrasives, which caused damage to local surface. However, owning to creep deformation of abrasives and interior controllable air pressure of pneumatic wheel, SCA method could not only ensure machining efficiency, but also avoid deep scratches as shown in Fig. 10d.

5.3 Influence of abrasive size

Usually, the final processing effect depended strongly on abrasive particle size. Therefore, for researching on effects of abrasive size, experimental conditions were shown in Table 4. Alundum was selected as abrasive and particle size was listed in Table 6. Machining experiments were carried out individually by free abrasives method and SCA method with the same size particles for 3 min.

Machining results indicated differences in material removal under different groups as shown in Fig. 11. From group *C* to group *F*, material removal of SCA machining apparently

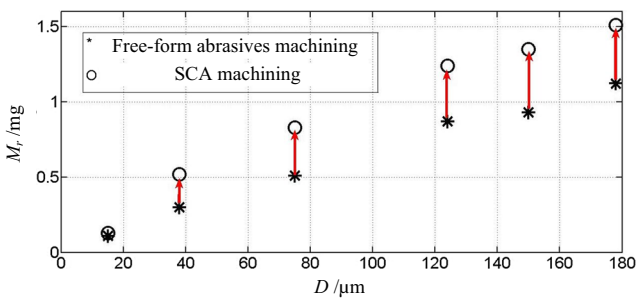

Fig. 11 Comparison on material removal

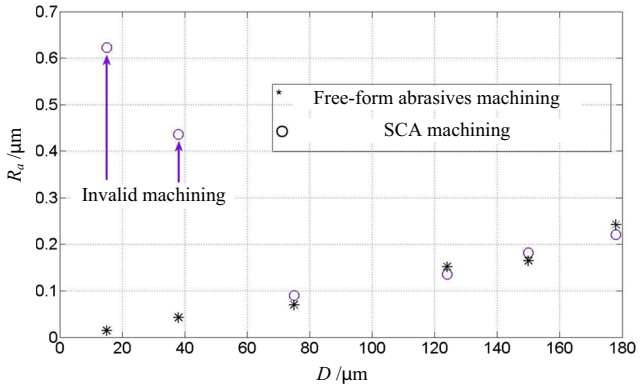

Fig. 12 Surface roughness R_a

exceeded that of free abrasives. However, improvement of machining efficiency with SCA was rarely evident in group *B* and group *A* shows the same machining low-efficiency between SCA method and free abrasives method.

After many repeated tests, it might be concluded that improvement of machining efficiency with SCA of particle diameter from 60 to 170 μm was obvious. Meantime, surface roughness was improved along with decrease of particle diameter. If particle diameter exceeded 170 μm, SCA were prone to cause deep scratches leading to decrease surface roughness. When particle diameter was lower than 60 μm, abrasives consolidation effect could be hindered by excessive small size of abrasive, which might lead to easy shaking-off of abrasives in machining process and weaken machining efficiency.

To research on surface roughness with SCA, initial R_a of 0.643 μm was processed under the experimental parameters as shown in Tables 4 and 5. Statistics of surface roughness were shown in Fig. 12.

When particle diameter exceeds 75 μm in the experiments carried out, free abrasives machining and SCA machining yield approximately identical R_a values. However, if particle diameter was less than 75 μm, SCA generally resulted in invalid machining. Figure 13 showed the respective machining effects with SCA of particle diameters of 38 and 75 μm.

It was obviously that machining effects in Fig. 13b (R_a=75 nm) was better than that in Fig. 13a (R_a= 482 nm). The major reason of different machining effects was that outer abrasives of SCA escape away with movement of wheel in machining process. It reduced major cutting area of SCA gradually. Without additional supplement of abrasives, machining of SCA would become vestigial by degrees. The above results reveal that SCA possess higher efficiency than free abrasives. To freeform surfaces, its flexibility can avoid damage which is always produced by rigid wheel. Meantime, SCA supplies high efficient material removal for high-hardness workpieces.

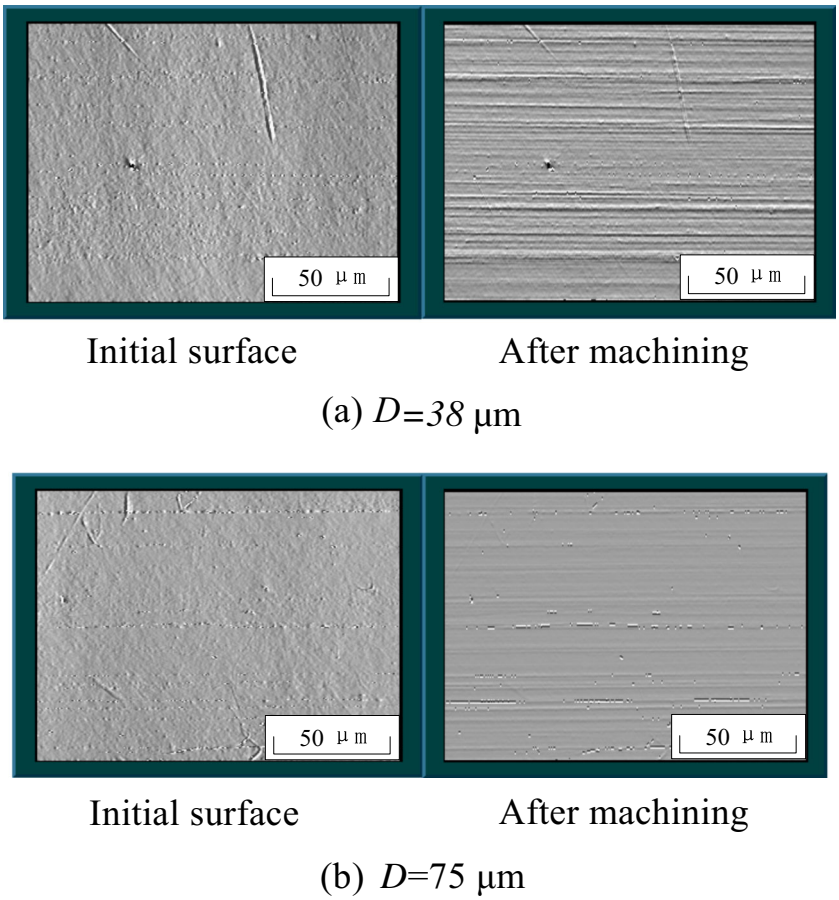

Fig. 13 Comparison of machining effects using abrasives of 38 μm diameters and abrasives of 75 μm diameters

6 Conclusions

To resolve problems in machining free-form surfaces of high hardness and high wear resistance efficiently, the paper analyzes mechanical characteristics of SCA and the following conclusions have been drawn via simulation and experiments.

1) In force chain of SCA, by utilizing soft ball model of abrasives and taking energy consumption into consideration, calculation method on normal and tangential force is given for analysis on contact model. Simulation results indicate that calculation error could be controlled within 1 %. Furthermore, it is concluded that damping coefficient of abrasives is vital factor for force transmission. SCA enjoys much denser force chain than free abrasives. Moreover it is likely to obtain higher efficient material removal effect.
2) Creep deformation of SCA is explained by simulation. According to global damping coefficient, the formulas of displacement and velocity of SCA are given in machining process. The creep deformation of SCA is confirmed in accordance with the velocity analysis of v_z of the single particle. Plenty of free abrasives have been confirmed to escape away in machining process. The simulation results indicate that the machining force of SCA enormously exceeds that of free abrasives.
3) Machining experiments on laser-hardened free-form surface has been carried out. The results show that material removal of SCA is higher than that of free abrasives by approximately 34.35 %. On the free-form surface, SCA also can avoid deep scratches which are always caused by rigid wheel. The comparison tests on abrasive size indicate that abrasives of smaller size (diameter less than 75 μm) are likely to fall away from SCA in machining process. Aiming to ensure both abrasives consolidation effect and machining efficiency, in SCA, abrasive size in a certain range (diameter from 75 to 150 μm) can help to improve material removal ability and control R_a within a range from 0.075 to 0.2 μm. In summary, SCA can be surely used in initial finishing processes to laser-hardened free-form surface.

Funding Authors acknowledge the financial support provided by the National Natural Science Foundation of China (51405444, 51175471, and 51205358). We also acknowledge the financial support of the Key Laboratory of Special Purpose Equipment and Advanced Manufacturing Technology Ministry of Education in Zhejiang University of Technology.

Conflict of interest The authors declare that they have no competing interest.

References

1. Qunli Z, Mykola A, Ruslan Z, Yi P, Volodymyr K, Yao JH (2012) Application of regression designs for simulation of laser cladding. Phys Procedia 39:92–97
2. Wang HM, Tang HB, Cai LX, Cao F, Zhang LY, Yu RL (2005) Microstructure and wear properties of laser clad Ti2Ni 3Si/Ni3Ti multiphase intermetallic coatings. Appl Phys A 80(8):1677–1682
3. Hong YC, Wang MH (2012) Research of microstructure and properties of Ni-based alloy hot sprayed-welding layers by laser remelted and aging treatment. Chinese J Mech Eng 48(10):75–81
4. Dandekar R, Chinmaya Y, Shin C (2013) Multi-scale modeling to predict sub-surface damage applied to laser-assisted machining of a particulate reinforced metal matrix composite. J Mater Process Technol 213:153–160
5. Kwok CT, Leong KI, Cheng FT, Man HC (2003) Microstructural and corrosion characteristics of laser surface-melted plastics mold steels. Mater Sci Eng A 357(1-2):94–103
6. Torkamany MJ, Sabbaghzadeh J, Hamedi MJ (2012) Effect of laser welding mode on the microstructure and mechanical performance of dissimilar laser spot welds between low carbon and austenitic stainless steels. Mater Des 34:666–672
7. Zeng X, Ji SM, Tan DP, Jin MS, Wen DH, Zhang L (2013) Softness consolidation abrasives material removal characteristic oriented to laser hardening surface. Int J Adv Manuf Technol 69:2323–2332
8. Yao CF, Wang T, Xiao W, Huang XC, Ren JX (2014) Experimental study on grinding force and grinding temperature of Aermet 100 steel in surface grinding. J Mater Process Technol 214(11):2191–2199
9. Sousa FJP, Hosse DS, Reichenbach I, Aurich JC, Seewig J (2013) Influence of kinematics and abrasive configuration on the grinding process of glass. J Mater Process Technol 213(5):728–739
10. Wu SH, Kazerounian K, Gan ZX, Sun YQ (2013) A simulation platform for optimal selection of robotic belt grinding system parameters. Int J Adv Manuf Technol 64(1-4):447–458
11. Song YX, Lv HB, Yang ZH (2012) An adaptive modeling method for a robot belt grinding process. IEEE ASME Trans Mechatron 17(2):309–317
12. Tsuneo K, Mitsuro H (2006) A study of EDM and ECM/ECM-lapping complex machining technology. Int J Mach Tools Manuf 14(46):1804–1810
13. Chiou YC, Lee RT, Yau CL (2007) A novel method of composite electroplating on lap in lapping process. Int J Mach Tools Manuf 47(2):361–367
14. Shi FG, Zhao B (1998) Modeling of chemical-mechanical polishing with soft pads. Appl Phys A 67(2):249–252
15. Han XS (2014) Investigation of the surface generation mechanism of mechanical polishing engineering ceramics using discrete element method. Appl Phys A 116(4):1729–1739
16. Ji SM, Jin MS, Zhang X, Zhang L, Zhang YD, Yuan JL (2007) Novel gasbag polishing technique for free-form mold. Chinese J Mech Eng 43(8):2–6
17. Kuriyagawa T, Saeki M, Syoji K (2002) Electrorheological fluid-assisted polishing for small three-dimensional parts. Precis Eng 26: 370–380
18. Suni J, Jain VK (2009) Rheological characterization of magnetorheological polishing fluid for MRAFF. Int J Adv Manuf Technol 42:656–668
19. Das M, Jain VK, Ghoshdastidar PS (2008) Analysis of magnetorheological abrasive flow finishing (MRAFF) process. Int J Adv Manuf Technol 38:613–621
20. Zeng X, Ji SM, Jin MS, Tan DP, Li JH, Zeng WT (2014) Investigation on machining characteristic of pneumatic wheel based on softness consolidation abrasives. Int J Precis Eng Manuf 2031–2039
21. Bi ZW, Sun QC, Liu JG, Jin F (2011) The quasistatic response of a granular matter to a localized loading. Mech in Eng 10–16
22. Ji SM, Li C, Tan DP, Yuan QL, Chi YW, Zhao LH (2011) Study on machinability of softness abrasive flow based on Preston equation. Chinese J Mech Eng 47(17):156–163
23. Ji SM, Zeng X, Jin MS, Tan DP (2013) New finishing method of softness consolidation abrasives and material removal characteristic analysis. Chinese J Mech Eng 49(5):173–181